Electronic Supplementary Material

Supplementary material for Gauthier *et al*. *Partitioning prediction uncertainty in climate-dependent population models.*

Methods

Population model

The probability to skip breeding (1 – breeding propensity) has been previously estimated [1] as the proportion of females that were not available for capture during the late summer banding drives, denoted *k*. However, these unavailable individuals include both the females that skipped breeding and those that lost all their eggs before hatching and subsequently migrated directly to distant moulting areas [2]. There is therefore a direct relationship between the parameter *k* estimated by van Oudenhove *et al*. [1], the probability of skipping breeding needed for our model ($\tilde{k}$), and the nest success parameter (v): $k = \tilde{k} + (1 - \tilde{k})(1 - v)$. We used this equation to feed our matrix models with estimates of the actual probability to skip breeding.

Introduction of a spring hunt in 1999 to control the population size had negative effects on components of fecundity due to hunting disturbance during spring staging: clutch size was reduced and age at first reproduction increased [1]. Previous studies of this population also reported a reduction of female breeding propensity following the spring hunt [3, 4], an effect that was not detected in the capture-recapture analysis of van Oudenhove *et al*. [1]. The transition from/to a state that is unobservable, here the non-breeding state, is notoriously difficult to estimate [5,6], leaving the possibility that an effect of spring hunt on probability of skipping breeding was masked by the large standard errors of parameter *k* estimated by van Oudenhove *et al*. [1]. Second, a previous analysis based on a state-space model found that, in order to reconstruct past population growth of our study population, the survival estimated from capture-

recapture-recovery data needed to be adjusted upwards [7]. This apparent bias in survival estimates could be due to mark loss, spatial heterogeneities in tag reporting rates or unknown sources of heterogeneity in either detection or survival probabilities [8,9]. To resolve these two issues (apparent lack of effect of spring hunt on probability of skipping breeding and downward-biased survival estimates), we adopted a model tuning approach in which we introduced four tuning parameters $\tau_1, \ldots, \tau_4$:

(1) $$logit\left(\tilde{k}^{(tuned)}(t)\right) = \begin{cases} logit\left(\tilde{k}(t)\right) & if\ t < 1999 \\ logit\left(\tilde{k}(t)\right) + \tau_1 & if\ t \geq 1999 \end{cases}$$

(2) $$S_0^{(tuned)}(t) = logit(a + (b + \tau_2) \cdot T(t)) \cdot \left(1 - logit(c + (d + \tau_3) \cdot H_0(t))\right)$$

with *a*, *b*, *c*, *d* as estimated from data

(3) $$logit\left(S_{1+}^{(tuned)}(t)\right) = logit(S_{1+}(t)) + \tau_4$$

We looked for the values of these tuning parameters that minimized the sum of squared errors between forecasted and observed population size over the period 1991-2011. The first two tuning operations were needed to reconstruct the plateauing of the population size after 1999 (Fig. S1, top left panel). The third tuning operation was needed to recreate the fast population increase before 1999. Tuning parameter values were respectively: 1.68 (meaning that the probability of skipping indeed increased after 1999 [3,4]), -1.45 (meaning that the temperature dependency in first-year survival was overestimated, cf. Fig. S1 bottom left panel), 0.44 (meaning that the relationship between harvest rate and first year survival was underestimated), and 0.59 (meaning that the adult survival rate was underestimated).

Auto-regressive moving-average models to project climate variability

We represented the inter-annual variability in weather realization under given climate scenarios (Step 4, Table 1) using auto-regressive moving-average models (ARMA). With this procedure,

we quantified both the level of autocorrelation and the amount of residual (independently and identically distributed) variance. We used those estimates to simulate scenario-specific random variation around the average temperature projections. We analysed the times series of projected temperature values for each of the 63 climate scenarios during each season between 1961 and 2080 (see section Climate scenarios below) to estimate the parameters of these ARMA models.

The objective was to derive multiple climatic projection time series for each scenario. Indeed, at all spatial scales, weather realizations under a particular climate are stochastic. To quantify this random variation, we ran auto-regressive moving-average models (ARMA) for each season- and scenario-specific average temperature time series between 1961 and 2080. The times series were first detrended. These models are described by their autocorrelation orders p and q, by the autocorrelation parameters θ and φ, and by the linear model parameters a, b, and σ, such that:

$$X_t = a + bt + \varepsilon_t + \sum_{i=1}^{p} \varphi_i X_{t-i} + \sum_{i=1}^{q} \theta_i \varepsilon_{t-i} \qquad \text{with} \quad \varepsilon_t \sim N(0, \sigma^2)$$

The orders p and q represent the time lags (in years) in the auto-regressive and moving-average parts of the models, respectively. Their value was selected between 0 and 6 using the Akaike Information Criterion (Table S1). For each temperature time series, we used those estimates to simulate scenario-specific random variation around the average temperature projections.

Simulation strategy

Here are some additional technical details regarding Step 6 of our simulations. For this step, we resampled in the approximate multivariate normal distribution of parameter estimates with the sampling variance-covariance matrix extracted from the analysis of van Oudenhove *et al*. [1]. However, this distribution is approximately correct only near the maximum likelihood parameter estimates and becomes increasingly incorrect away from these values. To avoid distortions

introduced by extreme and biologically unrealistic values, we capped the variation in the least precisely estimated parameters. Fecundity was thus bounded between 0.1 and 1.4 females per females, juvenile survival probability between 0.15 and 0.7, and the rate of accession to reproduction after age 4 constrained above 0.4. These biological boundaries were based on previous knowledge of the system. Not enforcing these boundaries and using the unmodified multivariate normal distribution to generate parameter values far from the maximum likelihood values yielded, among other unwanted features, an excess of pessimistic trajectories (population extinction] and a bimodal distribution of predicted population sizes.

Climate Scenarios

We selected 63 climate simulations to represent current expectations of future changes in anthropogenic greenhouse gas emissions and global circulations. From each simulation, daily region-specific scenarios were generated for 1) the core breeding area of greater snow geese in the eastern Canadian Arctic (between 68º-77ºN and 66º-95ºW), 2) spring and fall migration stopovers in southern Quebec (St-Lawrence Valley from the Ontario border in the west to the town of Rimouski to the east) and 3) wintering areas along the Atlantic coast of the US (between 35.5º-40ºN). For simulations with our population model, we averaged the daily temperature to get a single yearly temperature value for each scenario and each of the 3 regions; averages were performed only over days during which geese were present in the region, following van Oudenhove *et al*. [1].

A climate scenario is defined as a plausible future climate trajectory and is generally obtained by a post-processing method, which roughly consists in merging the observed historical climate with the future trends simulated by a numerical climatic model [10,11]. Climate change uncertainty is often discussed in terms of three different sources linked with, in order of

decreasing importance on the long term: anthropogenic greenhouse gas emissions, the diversity in model structures, and natural variability [12]. Post-processing also contributes to uncertainty in temperature scenarios but it can be minimized by forcing preservation of the simulated long-term trend (e.g. Grenier *et al*. [13]).

For this project, a set of 63 simulations from the Coupled Model Intercomparison Project phase 5 (CMIP5 [14]) generation global climatic models (GCMs) was selected (see Table S2 for the list of models). This ensemble represents 33 different GCMs and three of the four representative concentration pathways (RCPs; equivalent to emission scenarios [15]) currently used in climatology (RCP4.5, 6.0 and 8.5; RCP2.6 has been judged unrealistic). The selected simulations are identified by their GCM name and RCP forcing in Table S2. Prior to post-processing, daily values for each simulation and the related observational product were interpolated on a common 0.25^{o} x 0.25^{o} (latitude x longitude) grid within each region polygon, and then regionally averaged. The observational product for the Canadian regions is the 10 km x 10 km gridded dataset from Natural Resources Canada [16], whereas for the US region the National Oceanic and Atmospheric Administration (NOAA) td3200 and ds3200 datasets were used (NCDC-td3200) [17]. Each daily and regionally averaged simulation has been post-processed independently to construct a scenario, using a state-of-the-art technique. The central idea of the technique is to define a quantile-based transfer function between simulated and observed time series over a calibration period, and to then apply it to the entire simulation [11]. Each day of the year is treated specifically using a 31-day moving window, and only residuals around fourth-order long-term trends are treated in order to preserve the simulated long-trend trends. Calibration periods were 1961-2013 for the Canadian regions and 1961-2006 for the US region (more recent data were not available at the moment of doing the analysis). Quality control

was performed to ensure the input data and post-processing method were leading to plausible scenarios in terms of average annual cycles as well as annual mean, minimum and maximum of daily temperatures. Observed and projected temperature for each region and scenarios are shown in Fig. S2.

Theoretical exploration of prediction variance components

In this section we investigate analytically how the contribution of each source of uncertainty (Table 1) to the variance of the predicted population size varies with the prediction time horizon *t*. We make the following simplifying assumptions and approximations:

1. We consider a scalar model $n_{t+1} = u_t\, n_t$, where n_t is the population size in year *t*, rather than a full matrix model as presented in the main text. As long as the variation in age structure is not too strong from one year to the other, this approximation should be reasonable.
2. We neglect demographic stochasticity (Step 8 in Table 1), a reasonable approximation for large population size as it is the case of the greater snow goose.
3. Without loss of generality, we consider that the growth rate is related to a single covariate x_t, with unexplained residual environmental variation ε_t (Step 6 in Table 1).

The logarithm of the growth rate at time *t*, $\log(u_t)$, is linearized as a function of the covariate x_t:

Eq. A1 $$\log(u_t) = a + bx_t + \varepsilon_t$$

We denote y_t as the logarithm of the population size $\log(n_t)$. We then consider the sampling uncertainty in the estimates of the parameters a and b (represented in Step 7 in Table 1) and the uncertainty in the covariate (e.g. the variation in the covariates among years not represented in the climatic model, denoted as τ_t and encompassing both Steps 4 and 5 of Table 1).

Incorporating these sources of variance into Eq. A1, we obtain:

Eq. A2 $$y_{t+1} = y_t + \hat{a} + \hat{b}x_t + \hat{b}\tau_t + \varepsilon_t$$

Assuming the initial log population size y_1 is a non-random scalar, Eq. A2 can be reformulated as:

Eq. A3 $$y_{t+1} = y_1 + t\hat{a} + \hat{b}\sum_{i=1}^{t} x_i + \hat{b}\sum_{i=1}^{t} \tau_i + \sum_{i=1}^{t} \varepsilon_i$$

Since the two random variables $\hat{b}$ and $\sum_{i=1}^{t} \tau_i$ are independent and $E(\sum_{i=1}^{t} \tau_i) = 0$ by definition, we have:

Eq. A4 $$E\left(\hat{b}\sum_{i=1}^{t} \tau_i\right) = E(\hat{b})E\left(\sum_{i=1}^{t} \tau_i\right) = 0$$

We now introduce structural uncertainty in the demographic model (Step 3 in Table 1). It is represented by the biases δa and δb acting on parameters *a* and *b* respectively. These biases quantify the effect of using an inadequate model on parameter estimation. Combining Eq. A3 and A4 and incorporating the biases, we obtain:

Eq. A5 $$E(y_{t+1}) = y_1 + (a + \delta a) \cdot t + (b + \delta b) \cdot \left(\sum_{i=1}^{t} x_i\right)$$

leading to:

Eq. A6 $$y_{t+1} - E(y_{t+1}) = t(\hat{a} - a - \delta a) + \left(\hat{b} - b - \delta b\right)\sum_{i=1}^{t} x_i + \hat{b}\sum_{i=1}^{t} \tau_i + \sum_{i=1}^{t} \varepsilon_i$$

Simply rising Eq. A6 to the square and taking the expected value, we obtain:

Eq. A7
$$\mathrm{Var}(y_{t+1}) = E\left(t^2(\hat{a} - a - \delta a)^2 + \left(\hat{b} - b - \delta b\right)^2 \left(\sum_{i=1}^{t} x_i\right)^2 \right.$$
$$+ 2t(\hat{a} - a - \delta a)\left(\hat{b} - b - \delta b\right)\sum_{i=1}^{t} x_i + 2t(\hat{a} - a - \delta a)\hat{b}\sum_{i=1}^{t} \tau_i$$
$$+ 2\left(\hat{b} - b - \delta b\right)\sum_{i=1}^{t} x_i \sum_{i=1}^{t} \tau_i + \hat{b}^2 \left(\sum_{i=1}^{t} \tau_i\right)^2$$
$$+ 2t(\hat{a} - a - \delta a)\sum_{i=1}^{t} \varepsilon_i + 2\left(\hat{b} - b - \delta b\right)\sum_{i=1}^{t} x_i \sum_{i=1}^{t} \varepsilon_i$$
$$\left. + \left(\sum_{i=1}^{t} \varepsilon_i\right)^2 + 2\sum_{i=1}^{t} \tau_i \sum_{i=1}^{t} \varepsilon_i \right)$$

All but five terms in Eq. A7 are equal to zero, because the four terms in Eq. A6 are all independent from each other and the last three have an expected value of zero.

Now we denote as σ_a^2, σ_b^2 and σ_{ab} the sampling variances and covariance of the estimates of *a* and *b*. These variances and covariance do not incorporate the bias δa and δb caused by structural uncertainty in the demographic model. Eq. A7 can then be reformulated as:

Eq. A8
$$\mathrm{Var}(y_{t+1}) = t^2(\sigma_a^2 + \delta a^2) + \left(\sum_{i=1}^{t} x_i\right)^2 (\sigma_b^2 + \delta b^2) + 2t\left(\sum_{i=1}^{t} x_i\right)(\sigma_{ab} + \delta a \delta b)$$
$$+ t\sigma_\varepsilon^2 + \mathrm{Var}\left(\hat{b}\sum_{i=1}^{t} \tau_i\right)$$

Using the classical formula for the variance of a product of random variables (e.g. Mood et al. [18], pp. 178-179), we obtain:

Eq. A9
$$\mathrm{Var}\left(\hat{b}\sum_{i=1}^{t} \tau_i\right) = t(\sigma_b^2 + \delta b^2)\sigma_\tau^2 + t(b + \delta b)^2\sigma_\tau^2$$

and, in turn:

Eq. A10 $$\mathrm{Var}(y_{t+1}) = t^2\sigma_a^2 + \left(\sum_{i=1}^{t} x_i\right)^2 \sigma_b^2 + 2t\left(\sum_{i=1}^{t} x_i\right)\sigma_{ab} + t\sigma_\varepsilon^2 + t(\sigma_b^2+\delta b^2)\sigma_\tau^2 + tb^2\sigma_\tau^2$$

Substituting $t\bar{x}$ for $\sum_{i=1}^{t} x_i$ (even though x_i is not stationary in the case of climate change), Eq. A10 further simplifies to:

Eq. A11 $$\mathrm{Var}(y_{t+1}) = t^2 \cdot (\sigma_a^2 + \delta a^2 + \bar{x}^2\sigma_b^2 + \bar{x}^2\delta b^2 + 2\bar{x}\sigma_{ab} + 2\bar{x}\delta a\delta b) + t \cdot (\sigma_\varepsilon^2 + \sigma_b^2\sigma_\tau^2 + (b+\delta b)^2\sigma_\tau^2)$$

Eq. A11 clearly demonstrates the decomposition of the prediction variance into a quadratic form in the prediction time horizon *t*. The first component reduces to $t^2 \cdot MSE(\hat{a} + \hat{b}\bar{x})$, where MSE is a mean squared error (variance + bias²). It is thus directly linked to uncertainty in the demographic parameters, both through the sampling variance of the estimates and the structural uncertainty expressed as biases in the estimates. The second component grows as t, and is mostly linked to environmental variance, i.e., the uncertainty in the variation of the covariate among years and the unexplained environmental variation.

As the prediction time horizon increases, the quadratic term takes over the linear term. Eq. A11 therefore leads to the conclusion that, for long-term predictions of population size, uncertainty in the demographic model (Steps 3 and 7 in Table 1) should override uncertainty in the climate model (Steps 4-6 in Table 1). We reached the same conclusion empirically using simulations in the main text.

The quality and precision of the relationship in Eq. A11 depends on 1) the number of years in the study from which *a* and *b* are estimated, 2) the reduction of structural uncertainty in the demographic model, and 3) the dispersion of the values of the covariate x during the study period. This is a strong argument in favor of long term programs, as commonly developed for

vertebrate populations, and for continuing these programs in an era where the dispersion of the covariates is expected to increase because of climate change. One may also note that the variance is for the log population size, implying a quick divergence of the projection interval for the forecasted population size, as apparent in the simulations.

References

1. van Oudenhove L, Gauthier G, Lebreton J-D. 2014 Year-round effects of climate on demographic parameters of an arctic-nesting goose species. *J. Anim. Ecol.* **83**, 1322–1333.
2. Reed ET, Bêty J, Mainguy J, Gauthier G, Giroux J-F. 2003 Molt migration in relation to breeding success in greater snow geese. *Arctic* **56**, 76–81.
3. Mainguy J, Bêty J, Gauthier G, Giroux J-F. 2002 Are body condition and reproductive effort of laying greater snow geese affected by the spring hunt? *Condor* **104**, 156–162.
4. Reed ET, Gauthier G, Giroux J-F. 2004 Effects of spring conditions on breeding propensity of greater snow goose females. *Anim. Biodiversity Cons.* **27**, 35–46.
5. Souchay G, Gauthier G, Pradel R. 2014 To breed or not: a novel approach to estimate breeding propensity and potential reproductive trade-offs in an Arctic-nesting species. *Ecology* **95**, 2745–2756.
6. Schaub M, Gimenez O, Schmidt BR, Pradel R. 2004 Estimating survival and temporary emigration in the multistate capture-recapture framework. *Ecology* **85**, 2107–2113.
7. Gauthier G, Besbeas P, Lebreton J-D, Morgan, BJT. 2007 Population growth in snow geese: A modeling approach integrating demographic and survey information. *Ecology* **88**, 1420–1429.
8. Péron G, Crochet P-A, Choquet R, Pradel R, Lebreton J-D, Gimenez O. 2010 Capture-recapture models with heterogeneity to study survival senescence in the wild. *Oikos* **119**,

524–532.

9. Fletcher D, Lebreton J-D, Marescot L, Schaub M, Gimenez O, Dawson S, Slooten E. 2012 Bias in estimation of adult survival and asymptotic population growth rate caused by undetected capture heterogeneity. *Methods Ecol. Evol.* **3**, 206–216.
10. Themeßl MJ, Gobiet A, Heinrich G. 2012 Empirical-statistical downscaling and error correction of regional climate models and its impact on the climate change signal. *Climate Change* **112**, 449–468.
11. Gennaretti F, Sangelantoni L, Grenier P. 2015 Toward daily climate scenarios for Canadian Arctic coastal zones with more realistic temperature-precipitation interdependence. *J. Geophys. Res. Atmo.s* **120**, 11862–11877.
12. Hawkins E, Sutton R. 2009 The potential to narrow uncertainty in regional climate predictions. *Bull. Amer. Meteor. Soc.* **90**, 1095–1107.
13. Grenier P, de Elía R, Chaumont D. 2015 Chances of short-term cooling estimated from a selection of CMIP5-based climate scenarios during 2006–35 over Canada. *J. Climate* **28**, 3232–3249.
14. Taylor KE, Stouffer RJ, Meehl GA. 2012 An overview of CMIP5 and the experiment design. *Bull. Amer. Meteor. Soc.* **93**, 485–498.
15. van Vuuren DP *et al*. 2011 The representative concentration pathways: an overview. *Climatic Change* **109**, 5–31.
16. Hopkinson RF, McKenney DW, Milewska EJ, Hutchinson MF, Papadopol P,Vincent LA. 2011 Impact of aligning climatological day on gridding daily maximum–minimum temperature and precipitation over Canada. *J Appl Meteor. Climatol.* **50**, 1654–1665.
17. National Climatic Data Center/NESDIS/NOAA/U.S. Department of Commerce, National

Weather Service/NOAA/U.S. Department of Commerce, and Federal Aviation Agency/U.S. Department of Transportation. 1981, updated monthly. *Daily meteorological data for U.S. cooperative stations from NCDC TD3200.* Research data archive at the National Center for Atmospheric Research, Computational and Information Systems Laboratory. http://rda.ucar.edu/datasets/ds510.0/.

18. Mood AM, Graybill FA, Boes DC. 1974 *Introduction to the Theory of Statistics* 3rd ed. New York: McGraw-Hill.

Table S1. Values of the time lags (in years) selected by the auto-regressive and moving-average parts of the ARMA model (parameters *p* and *q*, respectively) for each of the 63 climate scenarios and for each time period of the snow goose annual cycle used in the demographic parameters vs temperature analyses.

Scenario #	Early summer in Arctic (20 Jun-20 Jul)		Late summer in Arctic (1 Aug-30 Sep)		Fall in Québec (1 Sep-30 Nov)		Winter in eastern USA (1 Dec-29 Feb)		Spring in Québec (1 Mar-31 May)		Spring in Arctic (10 May-20 Jun)	
	p	*q*	*p*	*q*	*p*	*q*	*p*	*q*	*p*	*q*	*p*	*q*
1	2	2	0	1	0	1	1	1	0	1	0	1
2	1	3	0	1	0	1	2	2	0	1	3	2
3	0	1	1	1	0	1	0	1	1	1	1	5
4	1	1	2	2	0	1	0	1	4	5	0	1
5	0	5	0	1	1	1	0	1	0	1	0	1
6	2	4	1	4	0	1	2	2	1	2	3	3
7	0	1	4	4	0	1	0	3	1	2	1	1
8	0	4	3	3	0	1	0	1	2	1	0	1
9	1	1	3	3	3	2	4	4	0	1	0	1
10	3	3	0	1	0	1	0	1	0	1	4	3
11	1	1	0	4	0	1	0	1	2	2	4	3
12	1	1	0	1	2	3	0	1	0	1	0	1
13	2	5	0	1	0	1	2	2	2	4	0	1
14	0	2	0	1	0	1	1	1	0	1	2	5
15	0	1	0	1	0	1	0	1	1	1	0	1
16	1	1	0	1	2	3	3	2	0	1	0	1
17	2	4	4	3	2	1	0	1	0	1	0	1
18	0	1	3	2	0	1	1	4	0	1	0	1
19	0	1	0	1	3	2	0	1	1	1	1	3
20	2	2	2	4	0	1	0	1	0	1	0	1
21	0	1	1	0	2	3	0	1	0	1	1	0
22	2	2	1	1	1	0	1	3	1	1	2	2
23	2	2	0	1	3	5	1	1	0	1	4	3
24	0	2	1	1	0	1	2	1	0	1	1	4
25	0	1	2	2	0	1	0	1	0	1	1	1
26	0	1	0	1	2	2	2	2	0	1	0	1
27	0	1	3	2	0	1	1	3	0	1	0	1
28	4	5	0	1	0	1	2	2	0	1	1	1
29	2	3	0	1	0	1	0	1	0	1	0	1
30	0	1	0	1	2	2	0	1	0	1	0	1
31	3	4	0	1	0	5	0	1	1	2	1	1
32	2	5	0	1	1	3	0	1	1	1	2	2

33	2	3	0	1	0	1	0	1	0	1	2	2
34	2	4	0	1	1	1	0	1	0	1	0	1
35	0	1	0	1	2	2	0	1	0	1	0	1
36	0	3	0	1	1	3	2	1	0	1	0	3
37	0	1	0	1	1	0	2	3	0	1	1	5
38	0	1	1	1	2	2	0	1	2	2	0	1
39	0	1	2	2	1	2	1	2	0	1	2	2
40	0	1	1	2	0	1	2	3	2	3	1	2
41	0	1	1	1	0	1	0	1	3	4	0	3
42	0	1	1	1	0	1	0	1	2	1	0	1
43	0	1	0	1	2	2	1	1	1	3	0	1
44	1	1	0	1	1	3	3	2	3	2	1	1
45	2	2	0	1	0	1	0	1	1	1	5	4
46	4	3	2	4	1	2	0	1	0	1	0	1
47	0	1	1	0	0	1	0	1	0	1	0	1
48	3	2	0	1	0	1	2	2	0	1	1	1
49	0	1	1	0	0	1	1	3	2	2	1	1
50	0	1	0	1	0	1	2	1	1	1	0	1
51	2	2	4	3	0	1	1	2	0	1	0	1
52	0	1	1	0	0	1	1	1	1	1	0	1
53	3	2	3	3	0	1	0	1	0	1	0	1
54	0	1	1	1	0	1	0	1	2	1	2	1
55	0	1	0	1	1	1	0	1	0	1	0	1
56	2	2	0	1	1	1	3	3	0	1	0	1
57	2	4	0	1	1	4	0	1	0	5	0	1
58	0	1	0	1	0	1	0	1	1	1	0	1
59	0	1	0	1	0	2	1	1	3	4	0	1
60	1	1	0	1	0	1	0	1	2	2	0	1
61	2	2	1	0	0	3	1	1	2	4	0	1
62	3	3	0	1	0	1	2	5	0	1	1	1
63	0	4	4	3	0	1	0	1	3	3	1	1

Table S2. Identification information for each numerical climatic model simulation post-processed to construct a scenario. Technical note: only model members with identification code r1i1p1 have been used in this study, except for simulation 30 (r6i1p1).

No	Climate model	Host country	Representative Concentration Pathway [1]
1	ACCESS1-0	Australia	RCP4.5
2	ACCESS1-0	Australia	RCP8.5
3	ACCESS1-3	Australia	RCP4.5
4	ACCESS1-3	Australia	RCP8.5
5	BNU-ESM	China	RCP4.5
6	BNU-ESM	China	RCP8.5
7	CCSM4	USA	RCP8.5
8	CMCC-CESM	Italia	RCP8.5
9	CMCC-CM	Italia	RCP4.5
10	CMCC-CM	Italia	RCP8.5
11	CMCC-CMS	Italia	RCP4.5
12	CMCC-CMS	Italia	RCP8.5
13	CNRM-CM5	France	RCP4.5
14	CNRM-CM5	France	RCP8.5
15	CSIRO-Mk3-6-0	Australia	RCP4.5
16	CSIRO-Mk3-6-0	Australia	RCP6.0
17	CSIRO-Mk3-6-0	Australia	RCP8.5
18	CanESM2	Canada	RCP4.5
19	CanESM2	Canada	RCP8.5
20	FGOALS-g2	China	RCP4.5
21	FGOALS-g2	China	RCP8.5
22	FGOALS-s2	China	RCP6.0
23	FGOALS-s2	China	RCP8.5
24	GFDL-CM3	USA	RCP4.5
25	GFDL-CM3	USA	RCP8.5
26	GFDL-ESM2G	USA	RCP4.5
27	GFDL-ESM2G	USA	RCP8.5
28	GFDL-ESM2M	USA	RCP4.5
29	GFDL-ESM2M	USA	RCP8.5

30	GISS-E2-R	USA	RCP4.5
31	IPSL-CM5A-LR	France	RCP4.5
32	IPSL-CM5A-LR	France	RCP6.0
33	IPSL-CM5A-LR	France	RCP8.5
34	IPSL-CM5A-MR	France	RCP4.5
35	IPSL-CM5A-MR	France	RCP6.0
36	IPSL-CM5A-MR	France	RCP8.5
37	IPSL-CM5B-LR	France	RCP4.5
38	IPSL-CM5B-LR	France	RCP8.5
39	MIROC-ESM	Japan	RCP4.5
40	MIROC-ESM	Japan	RCP6.0
41	MIROC-ESM	Japan	RCP8.5
42	MIROC-ESM-CHEM	Japan	RCP4.5
43	MIROC-ESM-CHEM	Japan	RCP6.0
44	MIROC-ESM-CHEM	Japan	RCP8.5
45	MIROC5	Japan	RCP4.5
46	MIROC5	Japan	RCP6.0
47	MIROC5	Japan	RCP8.5
48	MPI-ESM-LR	Germany	RCP4.5
49	MPI-ESM-LR	Germany	RCP8.5
50	MPI-ESM-MR	Germany	RCP4.5
51	MPI-ESM-MR	Germany	RCP8.5
52	MRI-CGCM3	Japan	RCP4.5
53	MRI-CGCM3	Japan	RCP6.0
54	MRI-CGCM3	Japan	RCP8.5
55	MRI-ESM1	Japan	RCP8.5
56	NorESM1-M	Norway	RCP4.5
57	NorESM1-M	Norway	RCP6.0
58	NorESM1-M	Norway	RCP8.5
59	bcc-csm1-1	China	RCP4.5
60	bcc-csm1-1	China	RCP6.0
61	bcc-csm1-1	China	RCP8.5
62	bcc-csm1-1-m	China	RCP4.5
63	bcc-csm1-1-m	China	RCP6.0

[1] RCPs may be viewed as an equivalent of what was termed “emission scenarios” prior to phase 5 of the Coupled Model Intercomparison Project (CMIP5). It represents the radiative forcing in

2100 due of anthropic origin; RCP4.5 = 4.5 W/m^2 (subjectively interpreted here as a low emission scenario), RCP6.0 = 6.0 W/m^2 (intermediate emission scenario), RCP8.5 = 8.5 W/m^2 (high emission scenario).

Table S3. Annual population size of greater snow geese obtained during the spring aerial photographic survey (source: [7] and J. Lefebvre, Canadian Wildlife Service, unpubl. data).

Year	Population size
1990	368 300
1991	352 600
1992	448 100
1993	498 400
1994	591 400
1995	616 600
1996	669 100
1997	657 500
1998	836 600
1999	1 008 000
2000	816 500
2001	837 420
2002	725 000
2003	678 001
2004	890 000
2005	880 000
2006	938 000
2007	1 019 420
2008	718 000
2009	1 009 000
2010	824 000
2011	917 000

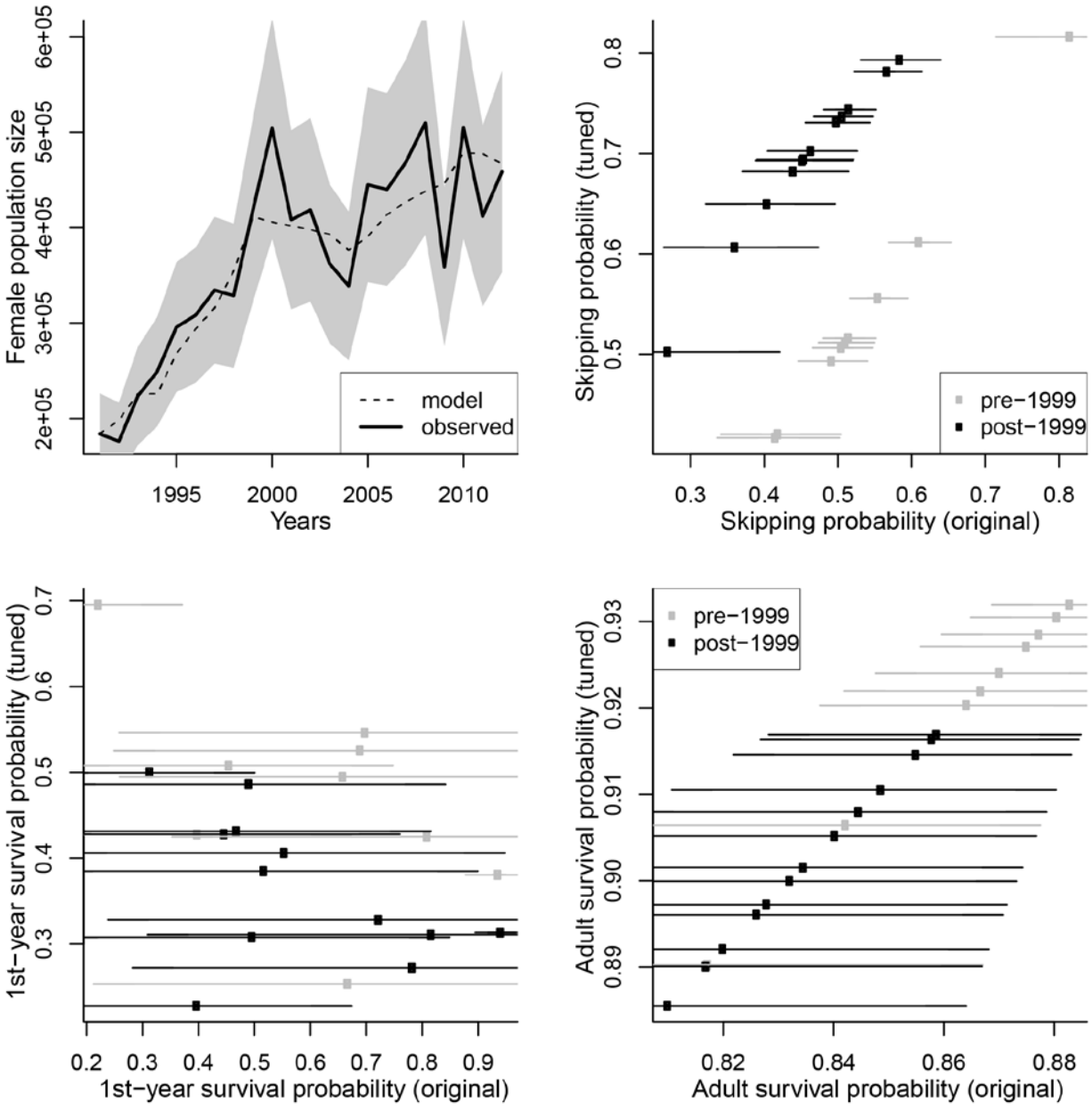

Fig. S1. Parameter tuning. Top left panel: population trajectory predicted by the tuned model (dashed line) laid over the observed fluctuations in population size (solid line, from Table S3, with 95% confidence interval in grey shading, from Gauthier *et al.* [7]). Top right panel: Relationship between the tuned and original probabilities to skip a breeding season (year-specific values). Lower panels: Relationship between tuned and original first-year survival probability (left) and survival probability for adults (right). Horizontal lines represent the standard error of

the parameter estimates before tuning. Grey symbols correspond to before 1999 (no special management measures, lower population size) and black symbols to after 1999 (special management actions including spring hunt, larger population size).

Fig. S2. Mean annual temperature (T_{mean}) in observations and the ensemble of 63 climate scenarios for each of the 3 major regions used by greater snow geese during their annual cycle (breeding range area, stopover area and wintering area). Observations cover 1961-2013 for breeding range and stopover areas, and 1961-2006 for wintering area; scenarios cover 1961-2080 for all areas. For each year, the average temperature values of the 63 scenarios were ranked, so that percentiles 10 and 90 (ranks 6 and 58) and 25 and 75 (ranks 16 and 48) could be determined, and the corresponding envelopes of temperature were displayed (scenarios could change ranks from year to year due to inter-annual variability).

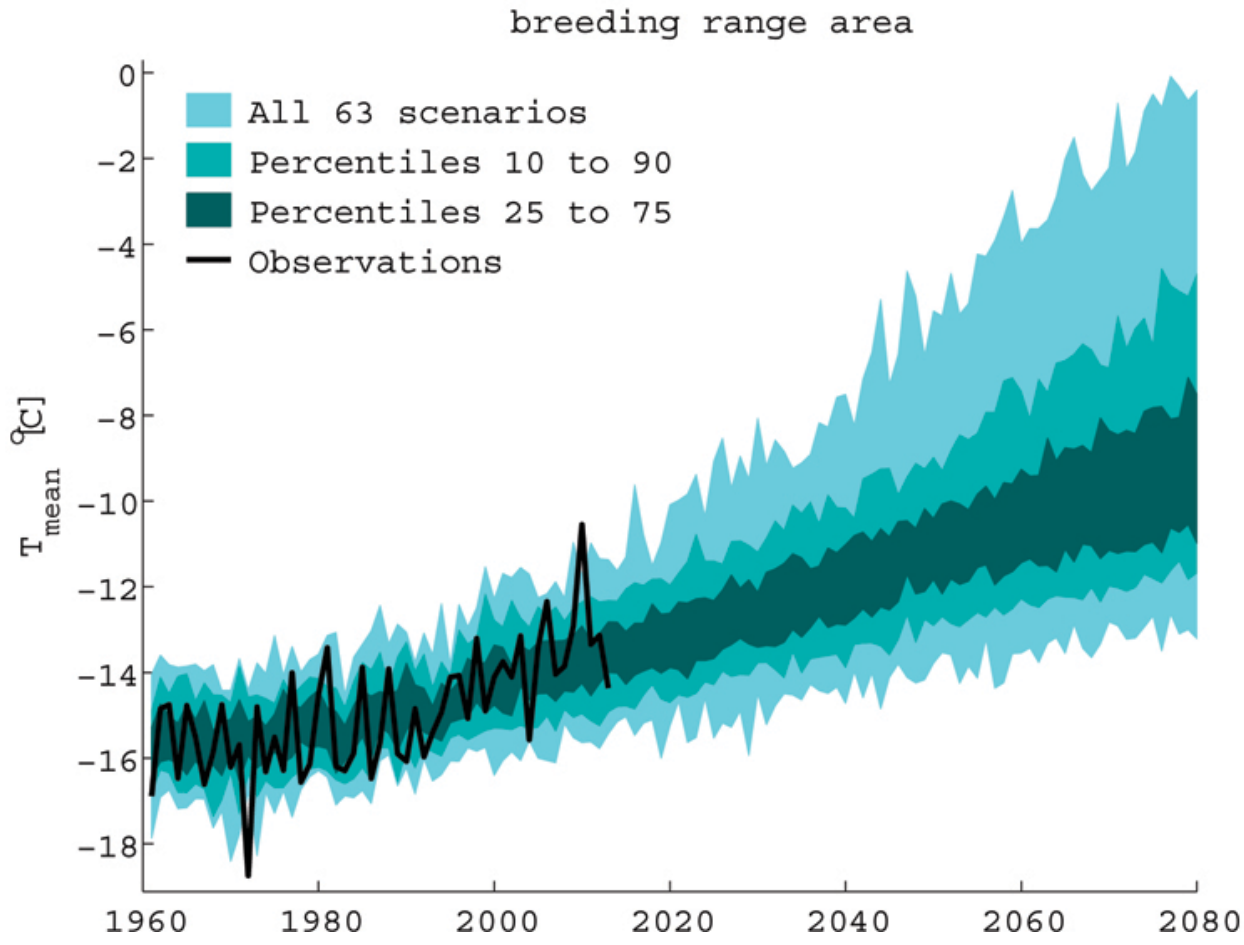

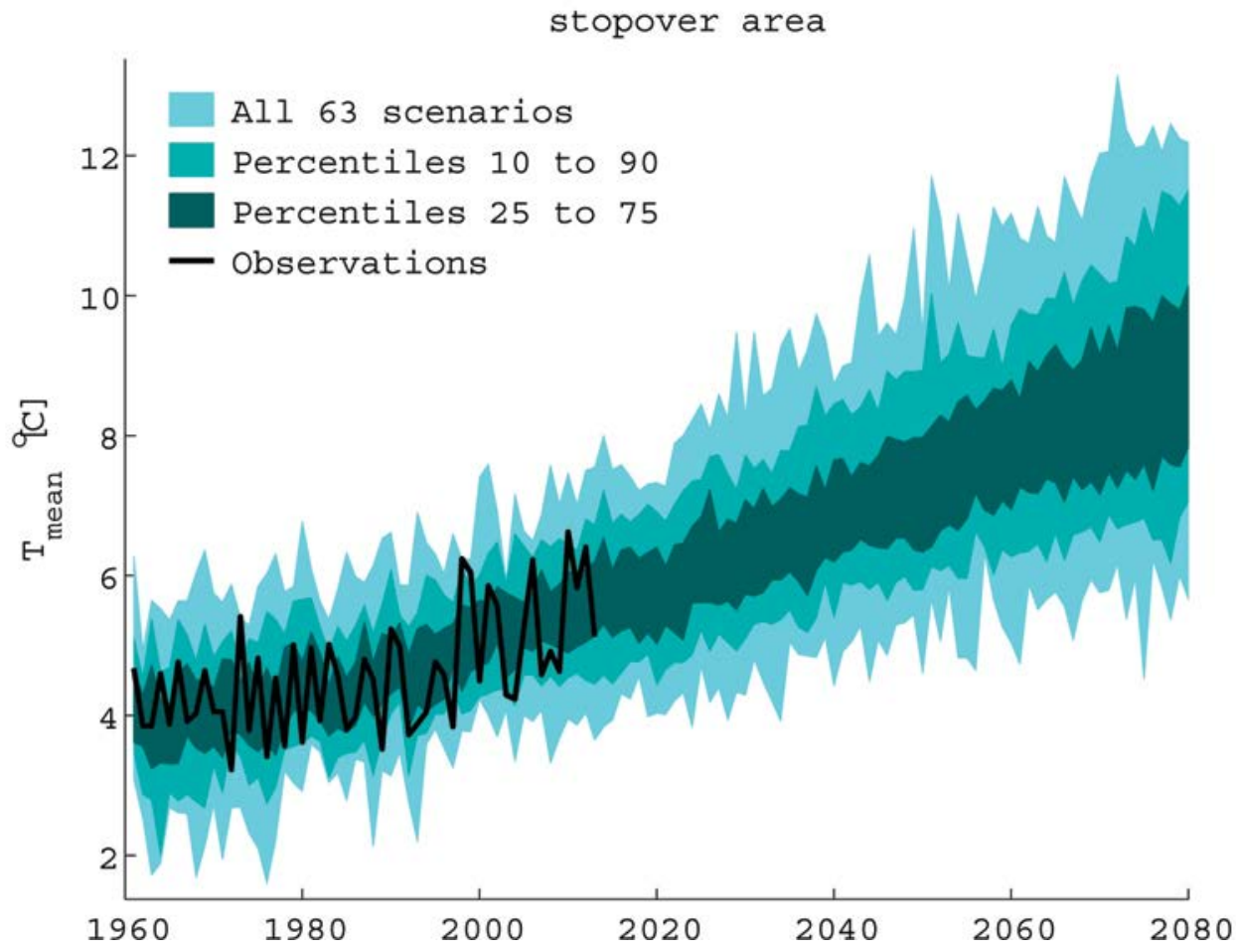
stopover area
All 63 scenarios
Percentiles 10 to 90
Percentiles 25 to 75
Observations
T mean °[C]
12
10
8
6
4
2
1960
1980
2000
2020
2040
2060
2080

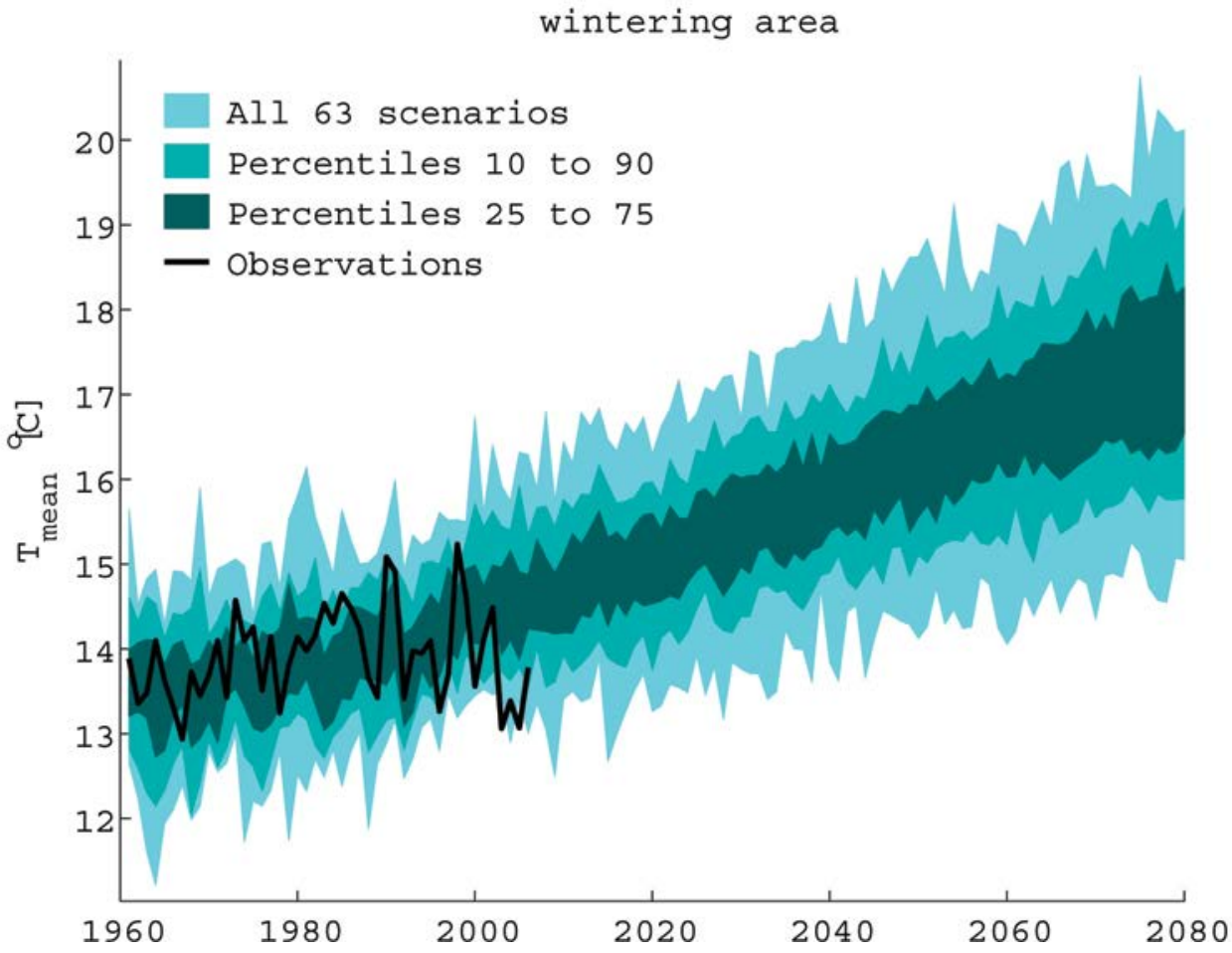
wintering area
All 63 scenarios
Percentiles 10 to 90
Percentiles 25 to 75
Observations
T mean [°C]
20
19
18
17
16
15
14
13
12
1960
1980
2000
2020
2040
2060
2080